Electrochemical and corrosion behavior of a 304 stainless-steel-based metal alloy wasteform in dilute aqueous environments

Jian Chen, R. Matthew Asmussen, Dmitrij Zagidulin, James J. Noël, David W. Shoesmith *

Department of Chemistry, Western University, London, Ontario, Canada N6A 5B7

ABSTRACT

The electrochemical and corrosion behavior of a stainless-steel-based alloy made as a prototype metallic nuclear wasteform to immobilize ^{99}Tc, has been studied in a number of reference solutions ranging in pH from 4 to 10. The results showed the 47SS(304)-9Zr–23Mo prototype alloy contained at least five distinct phases with the majority of the Re, used as a Tc surrogate, contained within a Fe_2Mo intermetallic phase. Polarization studies showed this alloy exhibited generally passive behavior in a range of dilute aqueous environments. Impedance measurements indicated passivity breakdown events can occur and lead to localized corrosion, especially in slightly alkaline conditions.

© 2012 Elsevier Ltd. All rights reserved.

1. Introduction

To meet the need for economic and sustainable nuclear energy production and to satisfy the requirements for controlled, proliferation-resistant nuclear materials management, fuel cycle technologies are under development to deal with the increasing inventory of spent nuclear fuel from commercial nuclear power plants [1–3]. The Department of Energy (DOE) in the USA is evaluating spent nuclear fuel processing options employing a range of aqueous-based and electrochemical processes [4]. Some of these waste streams could be efficiently accommodated in metal alloy waste forms. As part of the Fuel Cycle Research and Development (FCRD) program [5], Fe-based alloys are being developed and evaluated as potential waste forms [4,6–8].

A radionuclide of particular concern under waste disposal conditions is ^{99}Tc, a long-lived beta emitter produced by U fission in the fuel. This radionuclide potentially has a high mobility in oxidizing environments as pertechnetate (TcO_4^-). In the advanced UREX (Uranium Recovery by Extraction) separations process, a portion of the Tc inventory is extracted into the uranium recovery stream during fuel dissolution, in which it occurs as pertechnetate [9–11]. It is proposed that TcO_4^- can be separated from this stream, and reduced to be processed and immobilized as Tc metal, along with other transition metal fission product elements in an Fe-based [12,13] alloy. The development of an Fe-based waste form is being considered since the key high-melting temperature metallic elements (activation products like Tc, Mo, Ru, Pd, and Rh

that form the epsilon particles in the fuel [5,14]) present in various waste streams can be dissolved in molten Fe at a processing temperature of 1600 °C and then incorporated in durable intermetallic phases. Initial alloys were made to evaluate the approach by processing a surrogate waste mixture with reagent iron to identify (1) the phases that formed, (2) the distribution of Re (as an initial material for the alloy testing and development of the experimental techniques), and (3) the amount of iron that was required to accommodate the waste metals in durable intermetallics.

Previous studies have attempted to characterize the properties of metallic wasteforms based on stainless steel-zirconium formulations and their ability to act as hosts for Tc, noble metal fission products (e.g., Ru and Pd) and actinides (primarily U but also Pu and Np) [15–17]. Generally, corrosion evaluations were based on short term electrochemical and corrosion exposure tests [18–20]. In this paper the corrosion performance of stainless steel-based alloys has been assessed based on a combination of electrochemical and longer term corrosion experiments in order to assess their capacity to retain Tc and other radionuclides. The waste form under development is composed of several intermetallic phases with a minor amount of an iron solid solution phase. Prototype alloys have been made with Type 304L and Type 316L stainless steels. The results of tests and analyses conducted with the alloy made with Type 304L stainless steel are presented in this paper.

The primary goal of this work is to understand the degradation mechanisms of the component waste form alloy phases and how they influence the radionuclide release behavior under a wide range of exposure conditions. The larger program goal is to develop a model to predict the long term release of radionuclides (most importantly ^{99}Tc) under the range of environmental conditions

---

* Corresponding author. Tel.: +1 519 661 2111x86366; fax: +1 519 661 3022.
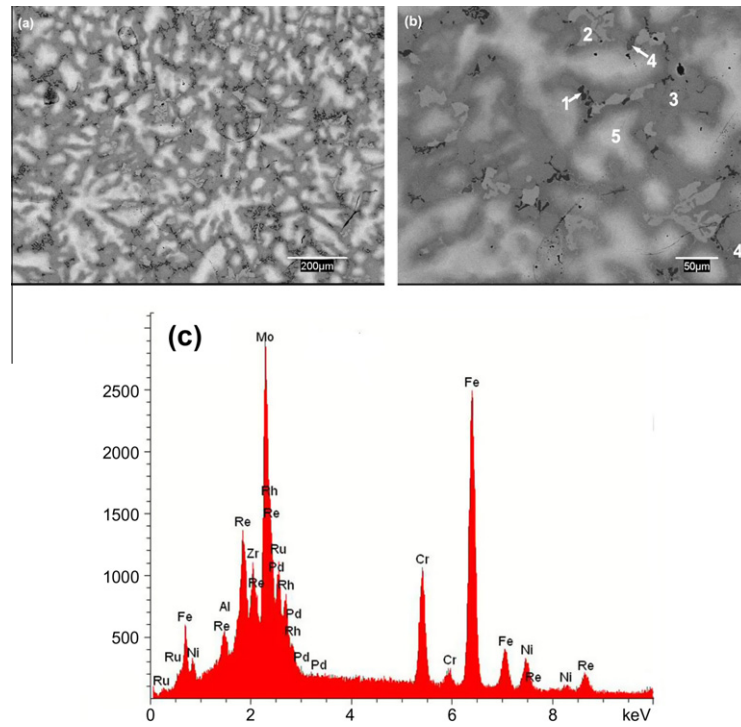*E-mail address:* dwshoesm@uwo.ca (D.W. Shoesmith).

Fig. 1. Microstructure and EDS analysis of Alloy 1: (a) low magnification; (b) high magnification; and (c) EDS area analysis.
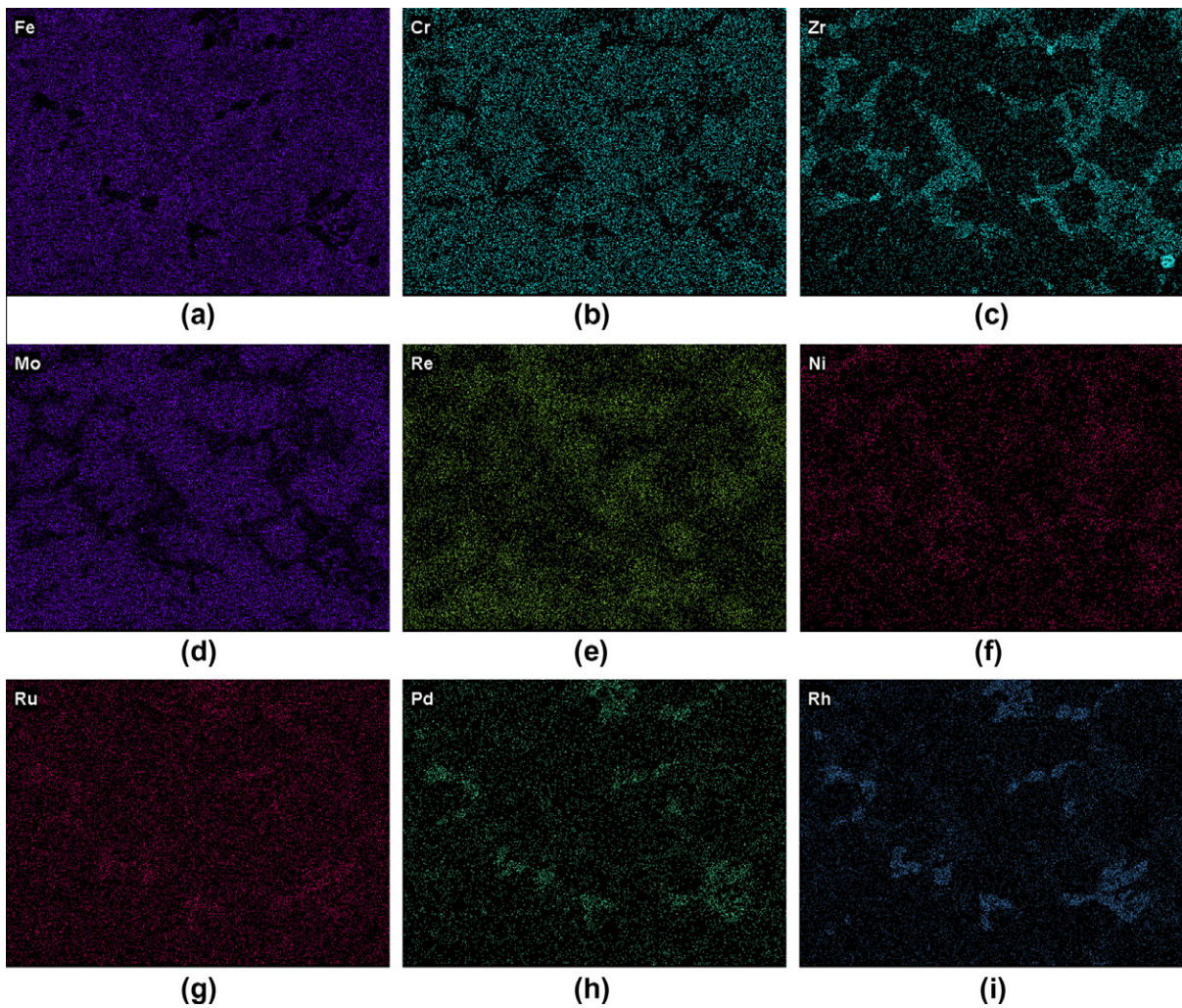

Fig. 2. Element distribution on the surface of Alloy 1 analyzed using EDS mapping (Fig. 1(b) shows the SEM image of this area on the same scale as the EDS maps).
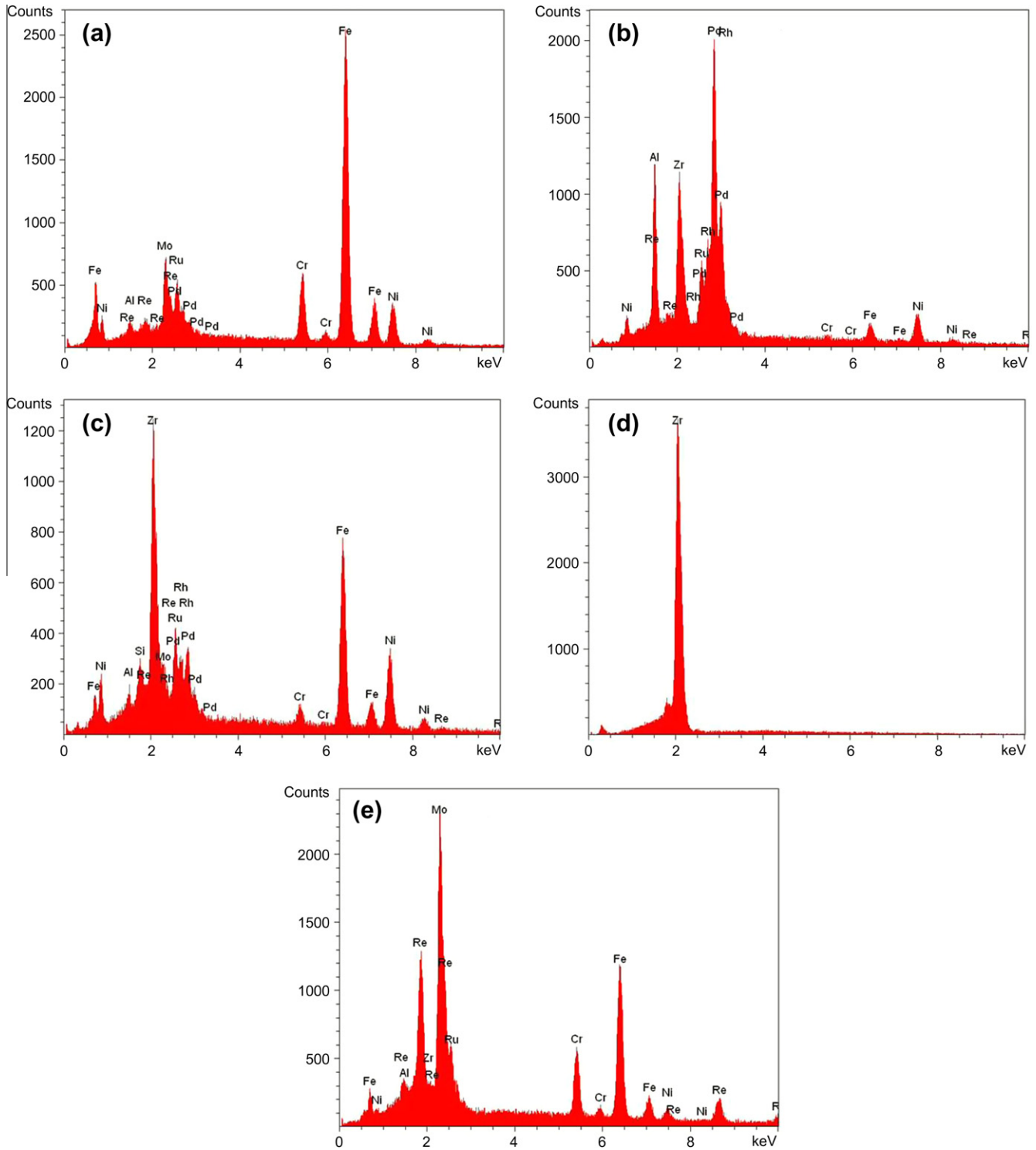
Fig. 3. EDS analyses of the marks in Fig. 2: (a) mark 1; (b) mark 2; (c) mark 3; (d) mark 4; and (e) mark 5.

which can provide source terms for waste disposal performance assessment models. This study concentrates on the development of an understanding of the general corrosion behavior of the multi-phase alloy in aqueous solutions with a range of pH and chloride concentrations, including the generation of passive layers and oxide films. Since the alloys contain multiple phases, it is likely that these films will differ from phase to phase leading to complex corrosion behavior.

2. Experimental

2.1. Sample preparation

Samples of the metal alloy were provided by Savannah River National Laboratory (SRNL). The preparation procedure has been described elsewhere [5]. The chemical composition of the 47SS(304)-9Zr–23Mo alloy (Alloy 1) (in wt.%) is Fe 32.79%, Cr
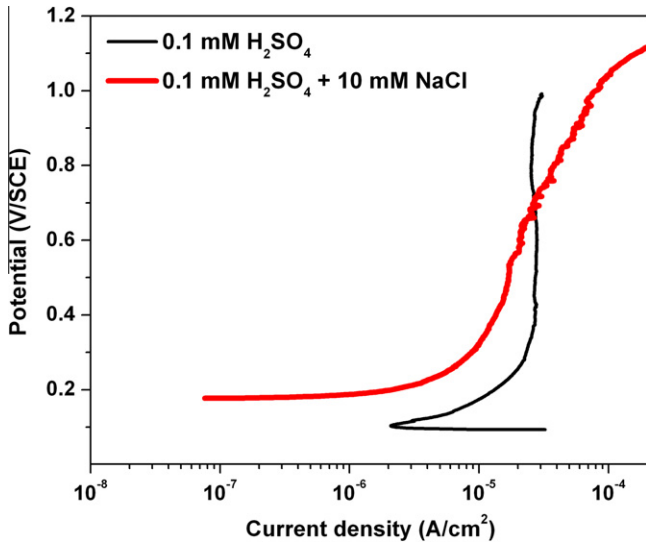
Fig. 4. Potentiodynamic curves of Alloy 1 in: 0.1 mM H_2SO_4 solution and 0.1 mM H_2SO_4 + 10 mM NaCl solution.

8.90%, Ni 5.15%, Zr 8.71%, Mo 22.25%, Re 10.18%, Ru 7.68%, Rh 1.12% and Pd 3.20%. The working electrodes were as-received cylinders, 0.5 cm by 0.2 cm in dimensions. The specimens were soldered to stainless steel, and a non-conductive lacquer painted on the sample to prevent contact of the stainless steel with the aqueous electrolyte. Once the paint was dry, the samples were put in an oven and heated at 60 °C for 12 h to promote the adhesion of the paint to the sample. The specimens were then ground successively with 240, 600, 800, 1000, 1200 grade SiC paper and then polished to a mirror finish using 1, 0.3, and 0.05 μm Al_2O_3 suspensions. The geometric area of the exposed surface was 0.196 cm². Prior to experiments, electrodes were washed with Type 1 water (obtained from a Milli-Q Academic system, with a resistivity of 18.2 MΩ cm), cleaned using methanol (reagent grade), washed again with Type 1 water, and finally dried using argon gas (ultra-pure grade).

2.2. Scanning electron microscopy (SEM) and energy dispersive X-ray spectroscopy (EDS) analysis

The morphologies of the surfaces were observed using a Hitachi S-4500 field emission scanning electron microscope (SEM) with a
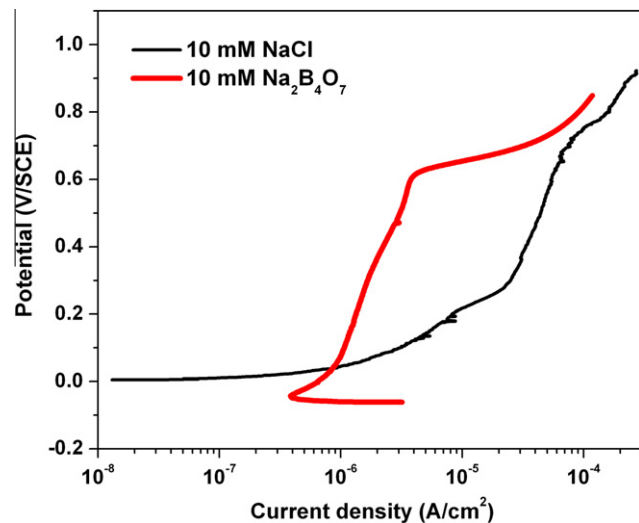
Quartz XOne energy dispersive X-ray spectroscopy (EDS) system. EDS analysis was used to characterize the elemental distribution within the metal waste alloys. To clearly identify the individual intermetallic phases, the surface was investigated using back scattered electron detection (BSE).

2.3. Electrochemical experiments

Experiments were conducted in a number of electrolytes covering a wide pH range with and without added sodium chloride: 0.1 mM H_2SO_4, 0.1 mM H_2SO_4 + 10 mM NaCl, 10 mM NaCl, 10 mM $Na_2B_4O_7$, 0.1 mM NaOH, and 0.1 mM NaOH + 10 mM NaCl. Solutions were prepared using Type 1 water, and reagent grade reagents: sulfuric acid (H_2SO_4, 18.4 M), sodium chloride (NaCl, 99.0% assay), sodium borate decahydrate ($Na_2B_4O_7 \cdot 10H_2O$, 99.5% assay), and sodium hydroxide (NaOH). All experiments were performed at ambient temperature, 22 ± 2 °C. Unless otherwise stated, the solutions were naturally aerated. This suite of solutions is being used to compare the durabilities of various materials under a wide range of conditions to ensure that the final waste forms will be suitable for use in various disposal environments.

Fig. 6. Potentiodynamic curves of Alloy 1 in: 0.1 mM NaOH solution and 0.1 mM NaOH + 10 mM NaCl solution.

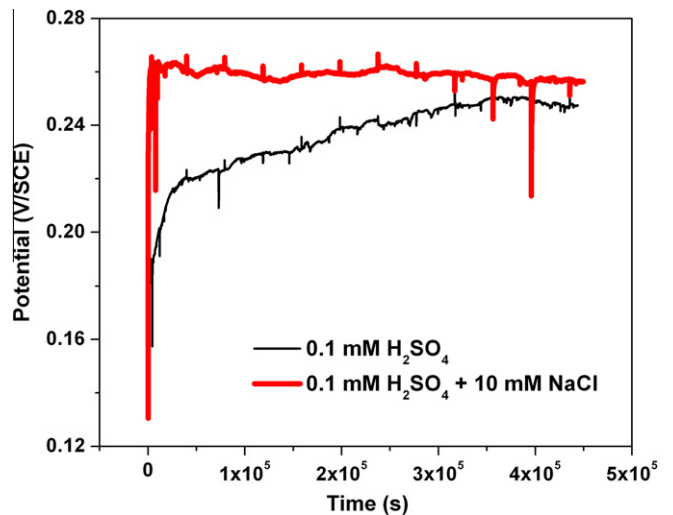**Fig. 5.** Potentiodynamic curves of Alloy 1 in: 10 mM NaCl solution and 10 mM $N_2B_4O_7$ solution.

Fig. 7. Evolution of corrosion potential for Alloy 1 in 0.1 mM H_2SO_4 solution and 0.1 mM H_2SO_4 + 10 mM NaCl solution with immersion time.
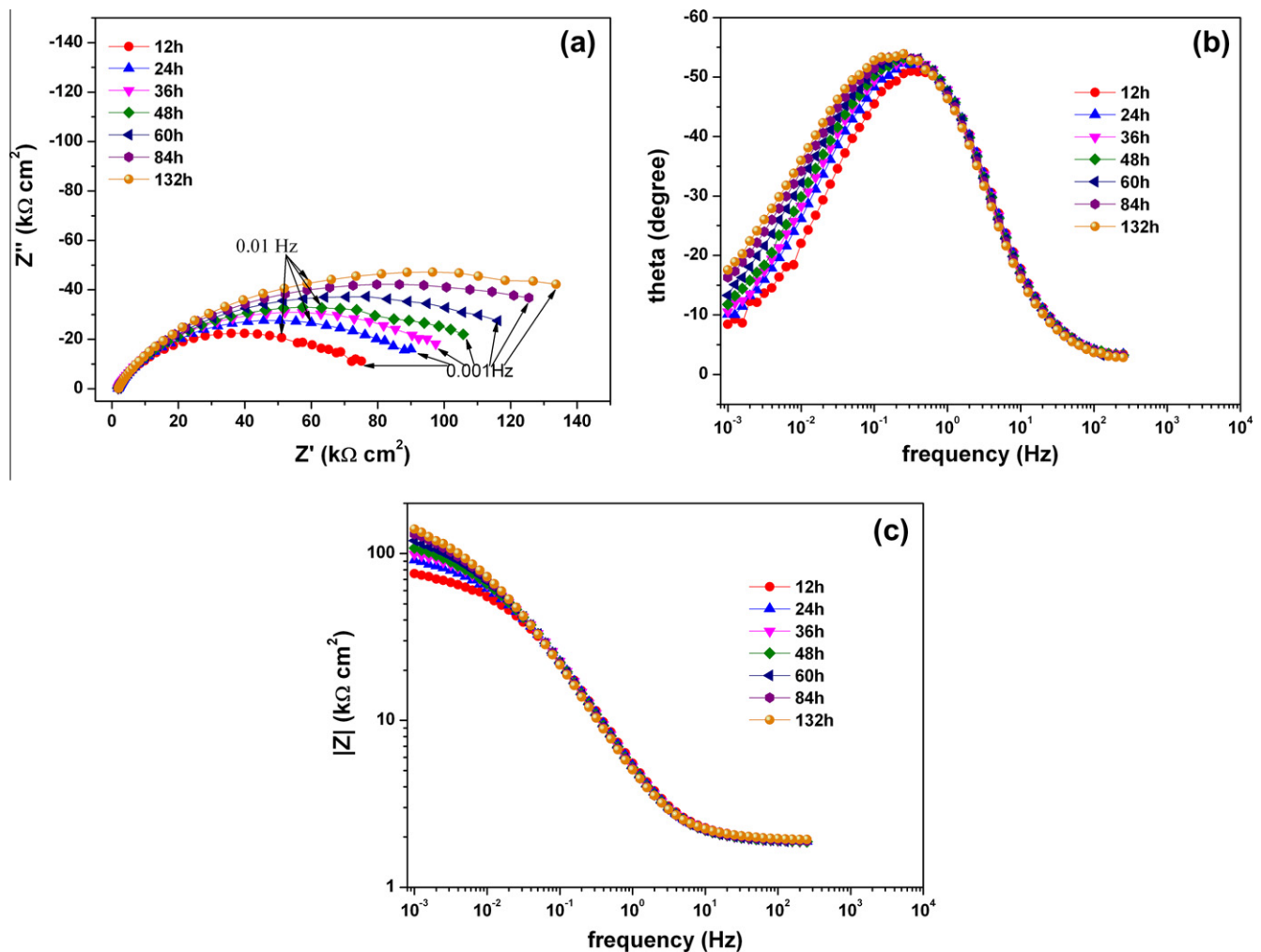
Fig. 8. Nyquist (a) and Bode (b) and (c) diagrams for Alloy 1 in 0.1 mM H_2SO_4 solution.

A standard three-electrode electrochemical cell was employed with the metal waste alloys as the working electrode, a Pt plate as the auxiliary electrode and a saturated calomel reference electrode (SCE) (−0.242 V/SHE). Electrodes were immersed in one of the six solutions for a sufficient period of time to establish a stable corrosion potential (E_{CORR}). The specimens were then cathodically cleaned at a potential 300 mV lower than E_{CORR} for 2 min, and then at a potential 150 mV lower than E_{CORR} for 2 min. Subsequently, potentiodynamic polarization curves were measured from E_{CORR} to 1.5 V/SCE at a scan rate of 0.167 mV/s.

To monitor the natural corrosion process, E_{CORR} was measured over a longer exposure period, and electrochemical impedance spectroscopy (EIS) measurements performed intermittently. Experiments were conducted in all six solutions using a Solarton 1287 electrochemical interface and a Solarton 1255B frequency response analyzer. EIS measurements were performed at E_{CORR} using a sinusoidal input potential with an amplitude of ±10 mV at individual frequencies over the range 10^5–10^{-3} Hz. Kramers–Krönig transformations of the experimental data were performed to ensure their validity.

3. Results and discussion

3.1. Microstructure

The microstructure observed using BSE and EDS analyses is shown in Fig. 1. A dendritic multiphase structure with an average dendrite size of ~200 μm (Fig. 1(a)) was observed. Amplification of the image suggests the presence of at least five phases (Fig. 1(b)). EDS analyses of the area detected all the alloying elements (shown below) including some aluminum oxide polishing residue, Fig. 1(c). EDS maps for the individual elements are shown in Fig. 2 and clearly demonstrate their segregation into distinct phases. Analysis of the EDS maps and spot analysis of different phases (Fig. 3) show the following: Phase 1, the black phase, is indistinguishable in the Fe map but deficient in the other main alloying elements, Mo, Cr, Zr and Re, with respect to the bulk composition; Phase 2, the white phase, is high in Zr, and the noble metals such as Pd and Rh, but deficient in Fe, Mo, Cr and Re; Phase 3 (the light grey phase) and Phase 4 (the grey phase) are dominated by Zr; Phase 5, the light phase, is dominated by the stainless steel elements Fe, Mo and Cr and rich in Re. The Ru and Ni appear quite generally distributed, although there is some suggestion the Ni is associated with the Zr dominated Phase 3. These observations indicate the material is predominantly a Fe–Mo–Cr-based Phase 5 containing the Re with lesser amounts of other phases, including the Fe-rich Phase 1, the Zr-based Phases 2 and 3 containing the noble metals Pd and Rh, and Phase 4, which is pure Zr.

Comparison of the microstructures and compositions of individual phases shows Alloy 1 is similar to the next generation prototype waste form alloy, the SS316 stainless-steel-based waste alloy RAW-1(Re) [21]. TEM results on RAW-1(Re) show the phase that is similar to Phase 1 in Alloy 1 to be an iron solid solution with a bcc structure [21]. EDS analyses of Phase 3 indicates that it is
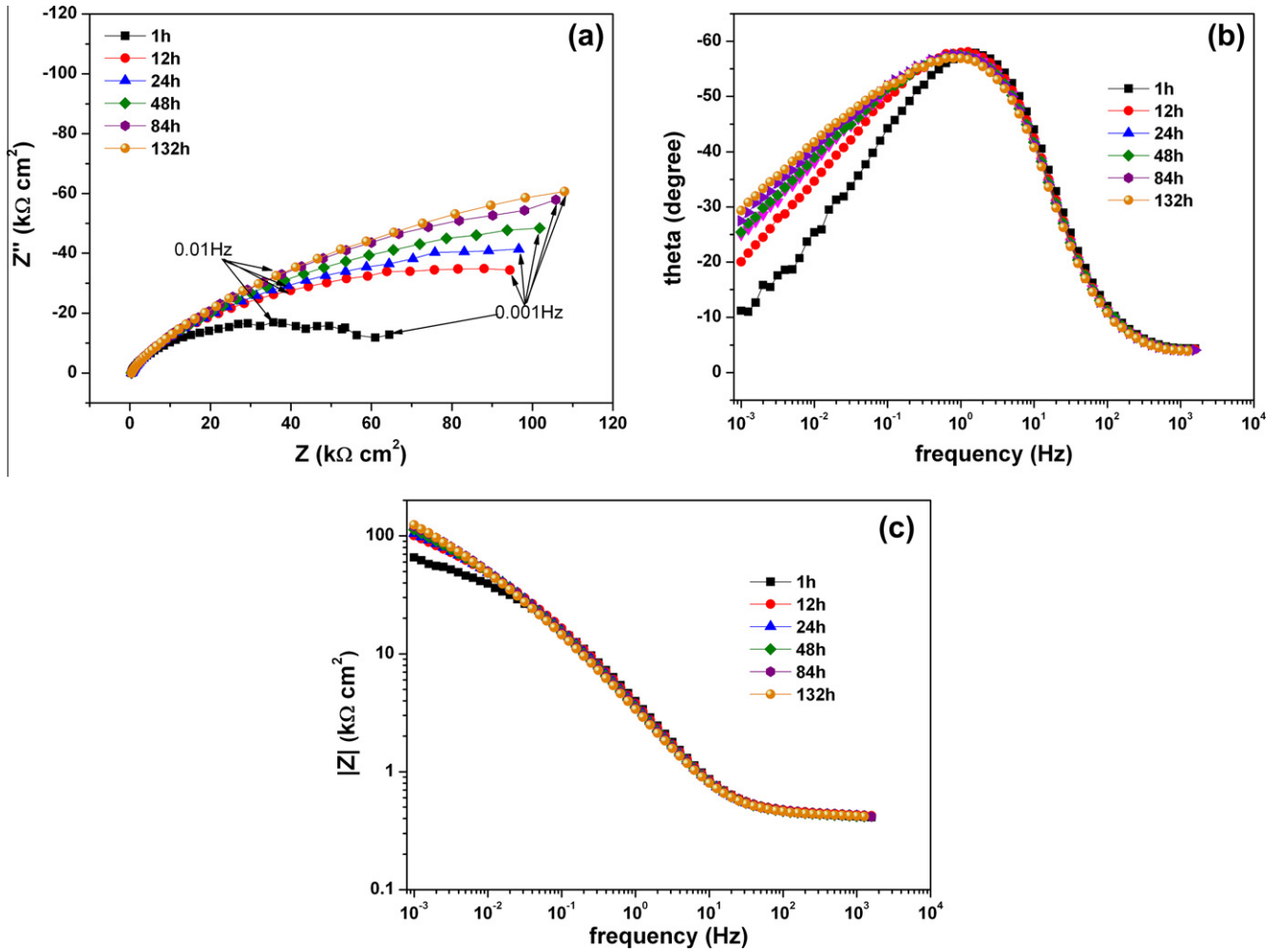
Fig. 9. Nyquist (a) and Bode (b) and (c) diagrams for Alloy 1 in 0.1 mM H_2SO_4 + 10 mM NaCl solution.

probably a Fe–Zr–Ni phase. Based on the microstructural analyses using TEM on RAW-1(Re), Phase 2 is probably a $(Ni,Fe)_2Zr$ intermetallic phase with a C15 cubic symmetry [21]. As indicated by the EDS spectrum in Fig. 3(e), Phase 5 is likely an Fe_2Mo intermetallic phase [21] and is the dominant host for Re.

3.2. Polarization behavior

The potentiodynamic polarization curves recorded in the six different naturally- aerated solutions are shown in Figs. 4–6. The curves exhibit similar features, with a passive potential range extending from the corrosion potential (E_{CORR}) to the onset of transpassivity, which usually occurs for potentials $\geqslant 0.5$ V/SCE. Generally, the passive currents are in the range 1 to 50 $\mu A\,cm^{-2}$, with currents up to one order of magnitude greater in acidic than in alkaline solutions, which is consistent with the generally observed behavior for stainless steels.

In the presence of chloride the current increases markedly at positive potentials. Usually this increase occurs at potentials >0.5 V/SCE suggesting the onset of transpassivity rather than localized film breakdown. In chloride-containing neutral solution, breakdown appears to occur at 0.2 V/SCE, Fig. 5, although the current increase is relatively minor. It is possible that uniform passivity is never achieved and the slow increases in current throughout the "passive" regions in acidic and alkaline solutions suggest this may be the case irrespective of solution pH.
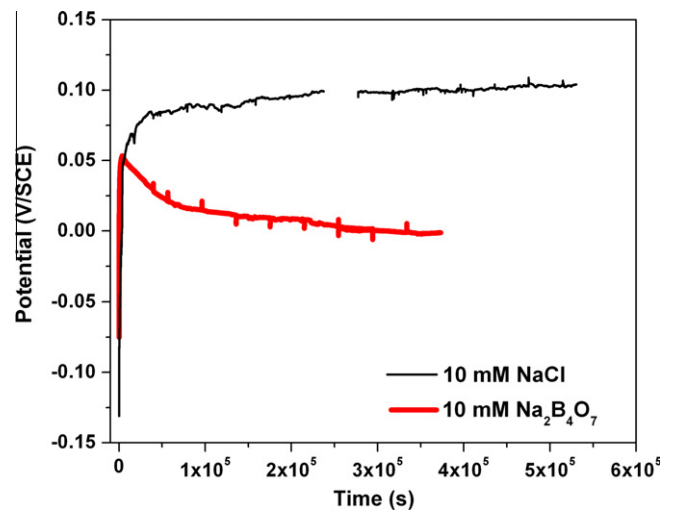

Fig. 10. Evolution of corrosion potential for Alloy 1 in 10 mM NaCl solution and 10 mM $Na_2B_4O_7$ solution with immersion time (we missed some data for a short period of time during E_{CORR} measurement in 10 mM NaCl solution).

3.3. Corrosion behavior

The longer-term corrosion process was followed for exposure periods up to 168 h and the reactivity of the surface monitored
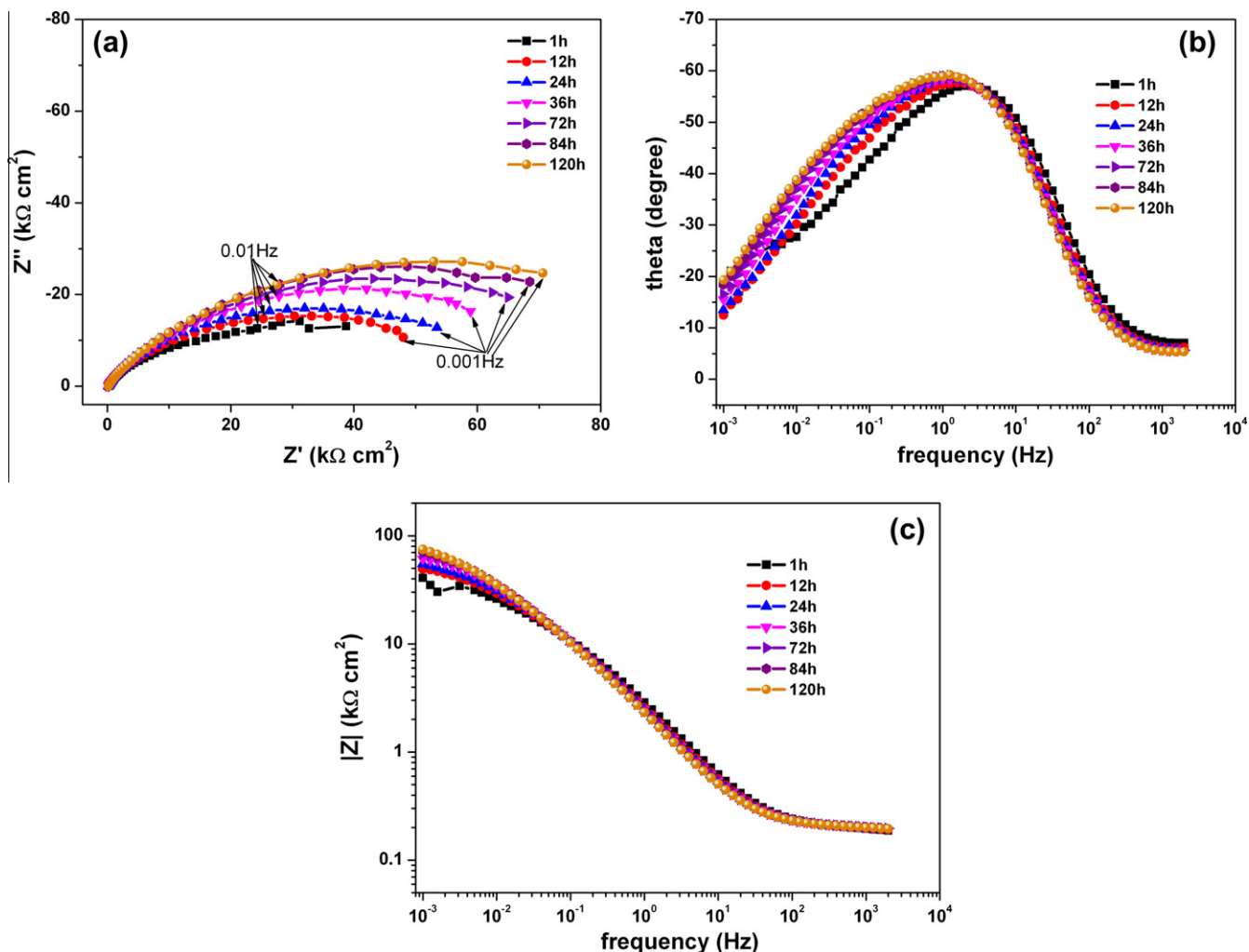
Fig. 11. Nyquist (a) and Bode (b) and (c) diagrams for Alloy 1 in 10 mM NaCl solution.

by EIS. EIS spectra recorded on such multiphase interfaces can only provide a general indication of surface behavior. This precludes any detailed interpretation of the spectra. Also, it is noted that the spectra (shown below) are inevitably distorted by frequency dispersion. This is not surprising given that the response of individual phase locations is unlikely to be the same.

Fig. 7 shows the evolution of E_{CORR} with immersion time in 0.1 mM H_2SO_4 solution and in 0.1 mM H_2SO_4 + 10 mM NaCl solution. In 0.1 mM H_2SO_4 solution, E_{CORR} increased to around 0.22 V/SCE over the first 10 h before subsequently increasing more slowly to ~0.25 V/SCE. Comparison of E_{CORR} to the polarization curve, Fig. 4, shows E_{CORR} is in the passive region. A series of EIS spectra recorded over the exposure period from 12 to 132 h is shown in Fig. 8. The Nyquist plot (Fig. 8(a)) exhibits only one capacitive loop indicating a single time constant response, Fig. 8(b), although it should be noted that the capacitative semicircle is flattened especially towards the low frequency limit. Irrespective of the complications introduced by this last feature, it is clear that the overall interfacial impedance is large ($\geqslant 10^5$ Ω cm^2 as the d.c. limit is approached) and increases with immersion time (Fig. 8(c)); i.e., the alloy interface is becoming generally more resistive suggesting a slow improvement in passive film properties. For immersion times >84 h the impedance spectra become effectively independent of time indicating that a condition of steady-state passivity was achieved.

The addition of chloride to the acidic solution does not lead to major changes in the E_{CORR} and EIS behavior, Figs. 7 and 9. E_{CORR} rises rapidly to the final steady-state value of ~0.26 V/SCE. Comparison to the polarization curve, Fig. 4, shows the potential to be marginally into the passive region. The EIS response at low frequencies, Fig. 9, confirms that, as in the absence of chloride, passivity develops steadily with increasing exposure time, eventually achieving a condition close to steady-state. There is some indication in the phase angle (Θ) vs. log (frequency) plot at low frequencies (10^{-2} to 10^{-3} Hz) of a second feature in the impedance data. A possibility is the diffusion of chloride within tight phase boundaries. Whether or not this could eventually lead to localized corrosion behavior remains undetermined.

In borate buffer, E_{CORR} initially rises to ~0.05 V/SCE before subsequently decreasing towards a lower steady-state value around 0 V/SCE (Fig. 10). By contrast, in the chloride solution, E_{CORR} rises rapidly to ~0.08 V/SCE and then slowly continues to increase to ~0.1 V/SCE, Fig. 10. According to the polarization curve, Fig. 5, this value is approaching the breakdown potential. However, EIS recorded in the chloride solution, Fig. 11, show a steady increase in interfacial impedance accompanies this long term increase in E_{CORR} and there is no evidence of film breakdown leading to localized corrosion. At longer times when E_{CORR} achieves a steady-state value the interfacial resistance (i.e., the interfacial impedance at the low frequency limit) is leveling out at a
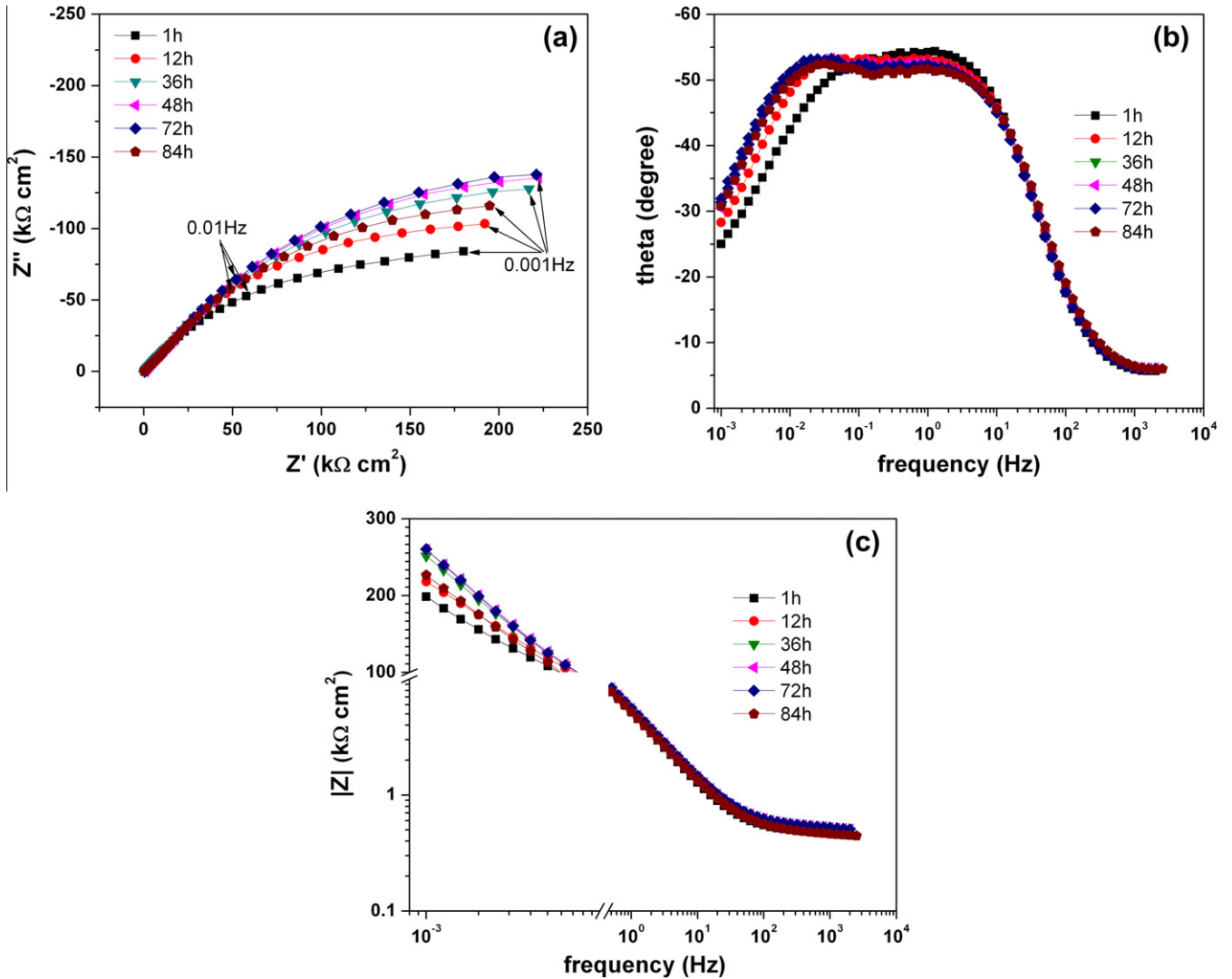
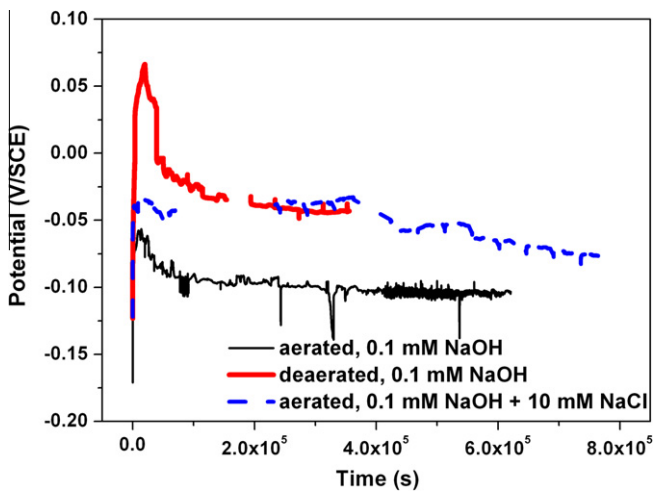**Fig. 12.** Nyquist (a) and Bode (b) and (c) diagrams for Alloy 1 in 10 mM Na$_2$B$_4$O$_7$ solution.

Fig. 13. Evolution of corrosion potential for Alloy 1 in 0.1 mM NaOH solution and 0.1 mM NaOH + 10 mM NaCl solution with immersion time.

value approaching ∼10^5 Ω cm^2 indicating a generally passive surface.

The EIS spectra recorded in 10 mM borate solution, Fig. 12, suggest that the decrease in E_{CORR}, Fig. 10, is accompanied by an initial small increase in interfacial impedance. This is inferred from the slight increase with time in the impedance (Z) observed at the lowest measurement frequency (Fig. 12c). However, at longer times the impedance decreases slightly as E_{CORR} achieves a steady-state value. In both sets of EIS spectra, Figs. 11 and 12, the plot of phase angle against log (frequency) shows the presence of two time constants, although the evidence is minor in the chloride solution. In the borate solution the two time constants become more distinct with increasing exposure time, Fig. 12(b), a slight decrease in phase angle at ∼10 Hz being accompanied by a slight increase at ∼10^{-2} Hz. How to assign these two time constants to specific processes for this multiphase alloy is unclear, but the increased prominence of the phase angle around 10^{-1} to 10^{-2} Hz accompanied by a small increase in impedance at low frequencies is indicative of a slight decrease in corrosion rate due to improved passivity. This would then suggest that the high frequency time constant is associated with more active behavior in fault sites within the generally passive matrix. The overall generally high impedance around 10 Hz indicates these fault locations are not particularly active, at least on the time scale of these experiments (up to ∼100–120 h). Given the multiphase nature of the alloy and the complicated interlacing of phases,
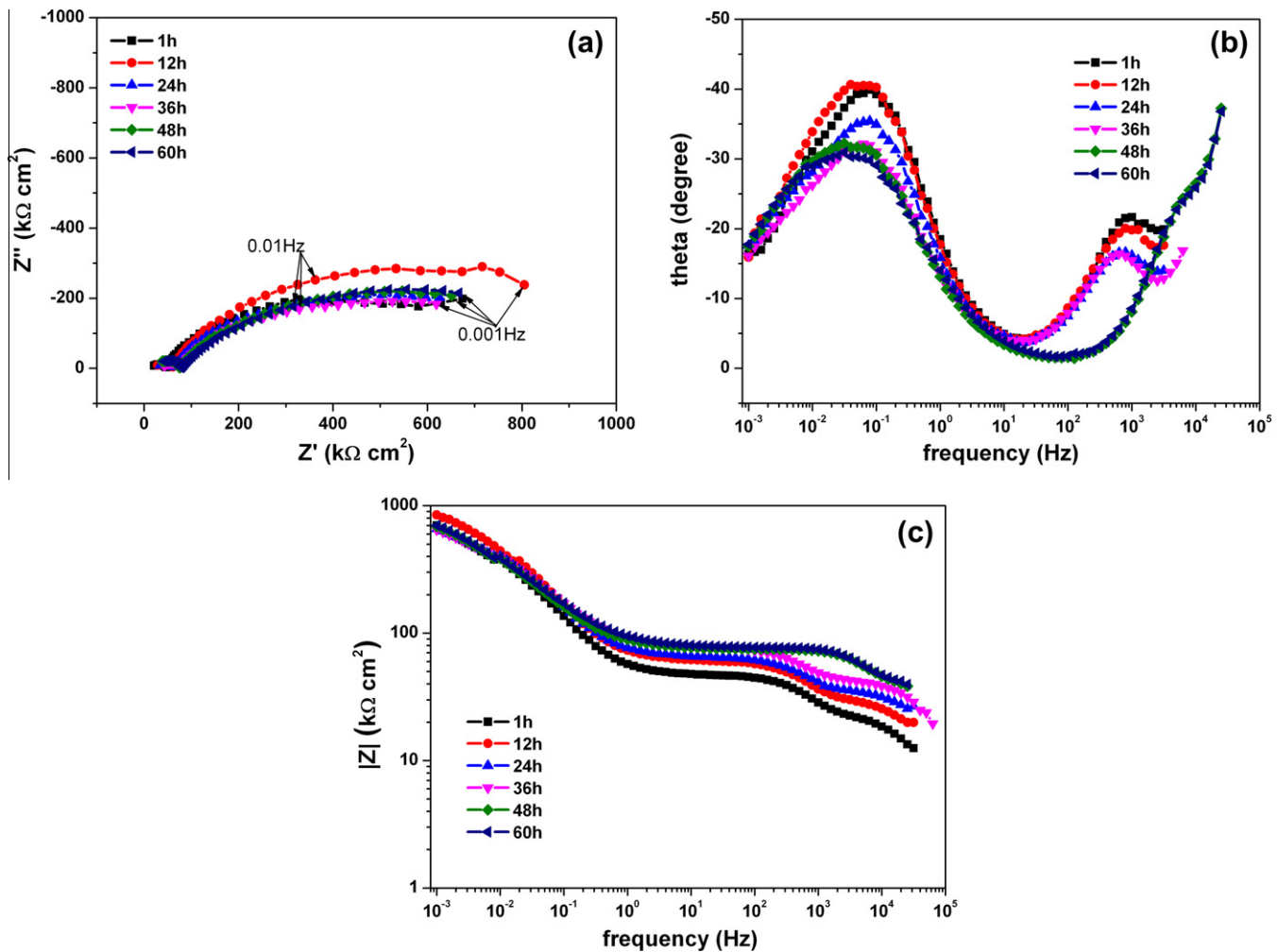
Fig. 14. Nyquist (a) and Bode (b) and (c) diagrams for Alloy 1 in 0.1 mM NaOH solution.

fault sites within phase boundaries would not be unexpected. That these sites appear to be more readily observed in neutral borate rather than neutral chloride solutions suggests they develop as a consequence of the alloy phase microstructure and are not primarily associated with chloride-induced breakdown processes.

In alkaline solution (0.1 mM NaOH), E_{CORR} rises initially to ~ -0.04 V/SCE before relaxing to ~ -0.1 V/SCE (Fig. 13). Such behavior, and a comparison to the polarization curve in Fig. 6 suggests this alloy may not be completely passive. E_{CORR} is noisy with a number of negative potential excursions suggesting possible metastable passive film breakdown events. The EIS behavior (Fig. 14) is also distinctly different to that observed in neutral and acidic solutions. Despite high frequency distortions of the impedance spectra at frequencies >10^3 Hz, two distinct impedance responses are observed, one at high frequencies ($\sim 10^3$ Hz) and a second at similar frequencies (10^{-1} to 10^{-2} Hz) to the responses observed in neutral and acidic solutions.

The overall impedance does not change much with time suggesting that there is no significant change in corrosion behavior with time and the high impedance observed as the low frequency limit is approached indicates a very low general corrosion rate. This suggests that the low E_{CORR} value and the high frequency response may be attributed to localized corrosion in exposed locations on an otherwise passive surface. According to the Pourbaix diagrams for the Mo–H_2O and Zr–H_2O systems [22], Mo and Zr tend to dissolve in alkaline solution. However, EDS analyses of

Alloy 1, Fig. 2, show that Mo always co-exists with Cr, which would preferentially be oxidized and form a stable oxide film [23] to protect Mo against oxidation. If so, these active locations may be associated with Zr-containing phases (Phases 2, 3 and 4, Fig. 2), probably at the boundaries with other phases [24], since Zr is considerably more soluble at pH = 10 than at pH = 4 or $\sim$7 [25], and hence the passive film would be more likely to dissolve.

Fig. 13 also shows the change in E_{CORR} with exposure time under deaerated (Ar-purged) conditions. The initial increase to positive potentials suggests an attempt to passivate before E_{CORR} relaxes to ~ -0.04 V/SCE. The difference in E_{CORR} between aerated and deaerated solutions indicates that whatever corrosion process is occurring is significantly polarized by the cathodic reduction of dissolved O_2. Whether or not this indicates that, due to the multiphase structure of the alloys, O_2 reduction at one location can stimulate localized dissolution at other remains to be investigated.

When chloride is present in the alkaline solution, E_{CORR} rapidly achieves a slightly more positive potential than in NaOH solution alone and shows only a very small relaxation to more negative values with time, Fig. 13. Some small negative-going transients are observed but are of minor amplitude compared to those observed in the absence of chloride. The EIS spectra, Fig. 15 shows almost no change with exposure time suggesting stable surface conditions. The absence of the high frequency response indicates the general absence of active behavior at local fault sites. As observed in the absence of chloride, the impedance, as the low frequency limit is
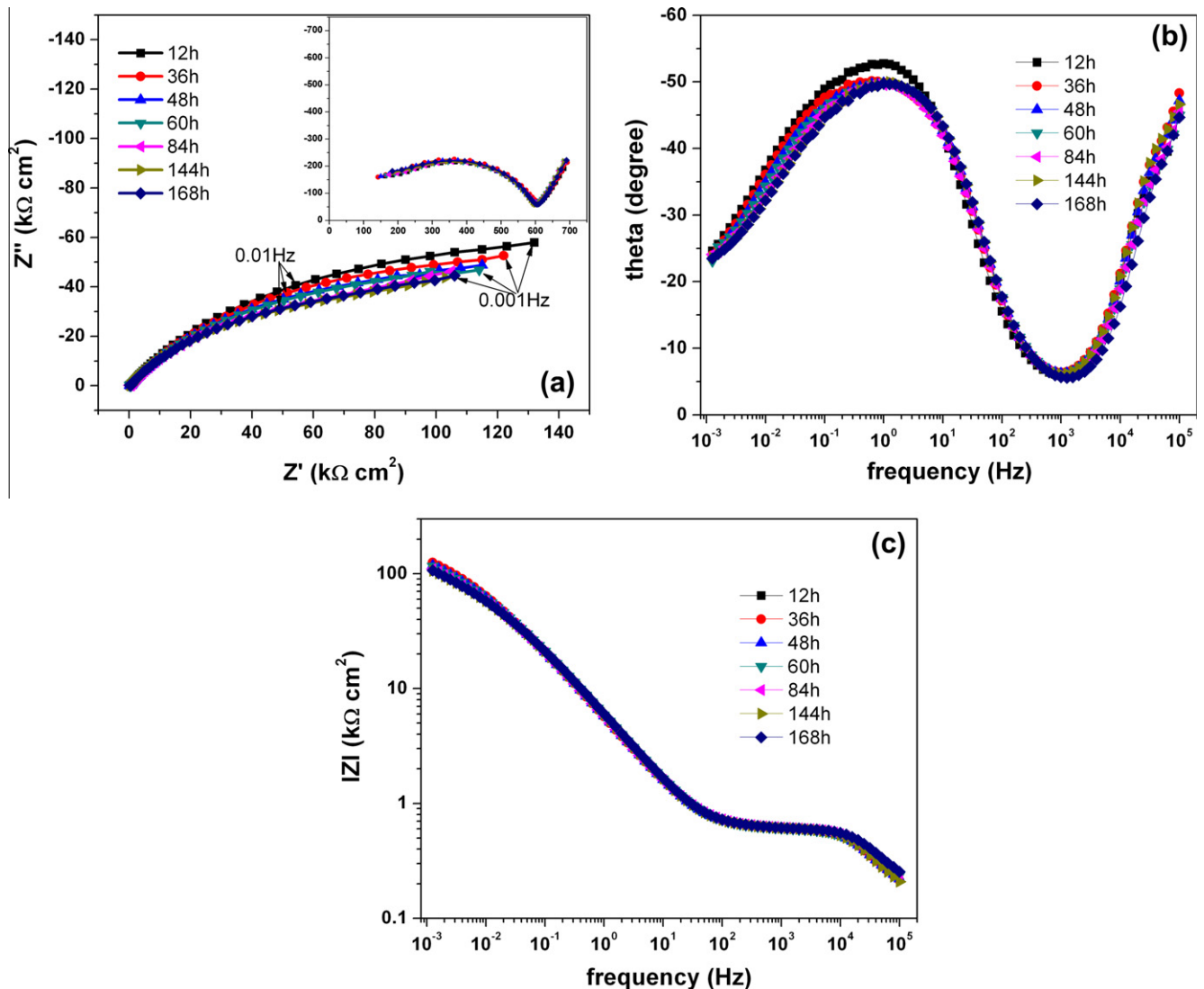
Fig. 15. Nyquist (a) and Bode (b) and (c) diagrams for Alloy 1 in 0.1 mM NaOH + 10 mM NaCl solution.

approached, is high indicating a low general corrosion rate. As concluded for neutral solutions these observations suggest that the presence of locally active sites is related more to microstructural features than chloride-induced breakdown.

4. Summary and conclusions

The electrochemical and corrosion behavior of a prototype stainless steel-based metallic nuclear waste form being designed to immobilize the radionuclide ^{99}Tc, has been studied in solutions ranging in pH from 4 to 10 with and without added NaCl. Scanning electron microscopy and dispersive X-ray spectroscopy showed that the 47SS(304)-9Zr–23Mo alloy contained at least five distinct phases, with the Re content primarily contained within an Fe_2Mo intermetallic phase. Polarization studies showed the alloy exhibited generally passive behavior in all solutions. Impedance measurements indicated potential passivity breakdown events leading to localized corrosion processes, especially in slightly alkaline conditions.

Acknowledgements

References

[1] R.A. Levich, J.S. Stuckless, Yucca Mountain, Nevada – a proposed geologic repository for high-level nuclear waste, Geol. Soc. Am. Memoirs 199 (2007) 1–7.
[2] J.R. Dyer, M.D. Voegel, The Yucca Mountain site characterization project in the United States, Lawrence Berkeley National Laboratory, Report LBNL-49767, 2001.
[3] http://www.ne.doe.gov/AFCI/neAFCI.html (August 29, 2012).
[4] D. Gombert II, R. Counce, V. Maio, A. Cozzi, J. Marra, J.V. Crum, T. Nenoff, W. Ebert, R. Scheele, C. Jantzen, H. Smith, J. Jerden, B. Spencer, R. Jubin, D. Strachan, M. Kaminski, J. Vienna, Global nuclear energy partnership integrated waste management strategy waste treatment baseline study, vol. I, September 2007, GNEP-WAST-AI-RT-2007-000324.
[5] M.J. Williamson, R.L. Sindelar, Development of an Fe-based alloy waste form for spent nuclear fuel, Savannah River National Laboratory, 2009, AFCI-SEPA-WAST-MI-DV-2009-000143/SRNL-STI-2009-00522.
[6] D.P. Abraham, L.J. Simpson, M.J. Devries, S.M. McDeavitt, Corrosion testing of stainless steel–zirconium metal waste forms, Mat. Res. Soc. Symp. Proc. 556 (1999) 945.
[7] D.D. Keiser, W. Sinkler, D.P. Abraham, J.W. Richardson, S.M. McDeavitt, The effects of actinides on the microstructural development in a metallic high-level nuclear waste form, Argonne National Laboratory, ANL/NT/CP-100293, 1999.

[8] D.P. Abraham, S.M. McDeavitt, J. Park, Metal waste forms from the electrometallurgical treatment of spent nuclear fuel, Argonne National Laboratory, ANL/CMT/CP-88008 CONF-9606116-14, 1996.

[9] N.C. Shroeder, M. Attrep, T. Marrero, Technetium and Iodine Separations in the UREX Process, Los Alamos, NM, 2001, Los Alamos National Laboratory Report: LA-UR-01-6607, 1996.

[10] G. Uchiyama, T. Asakura, S. Hotoju, H. Mineo, K. Kamei, M. Watanabe, S. Fujine, Solvent extraction behavior of minor nuclides in nuclear fuel reprocessing process, J. Radioanal. Nucl. Chem. 246 (2000) 683–688.

[11] V.S. Koltunov, V.I. Marchenko, A.S. Nikiforov, V.S. Smelov, V.S. Schmidt, T.V. Gomonova, A.K. Polunin, B.A. Kondra'ev, The role taken by technetium in the oxidation-reduction processes used in irradiated fuel technology, Atomnaya E' nergiya (trans) 60 (1986) 43–51.

[12] W.L. Ebert, M.A. Lewis, S.G. Johnson, Monitoring the consistency of multiphase waste forms, in: American Nuclear Society, Reno, NV, 2007, 11/11-15/01.

[13] W.L. Ebert, Testing to evaluate the suitability of waste forms developed for electrometallurgically treated spent sodium-bonded nuclear fuel for disposal in the Yucca Mountain repository, Argonne National Laboratory, September 2005, ANL-05/43.

[14] W.L. Ebert, M. Williamson, S. Frank, Immobilizing Tc-bearing waste streams in an iron-based alloy waste form, Argonne, Savannah River, and Idaho National Laboratories, September 2009, AFCI-WAST-PMO-MI-DV-2009- 00160.

[15] S.M. McDeavitt, D.P. Abraham, J.Y. Park, Evaluation of stainless steel–zirconium alloys as high-level nuclear waste forms, J. Nucl. Mater. 257 (1998) 21–34.

[16] D.D. Keiser Jr., D.P. Abraham, J.W. Richardson Jr., Influence of technetium on the microstructure of a stainless steel–zirconium alloy, J. Nucl. Mater. 277 (2000) 333–338.

[17] D.D. Keiser Jr., D.P. Abraham, W. Sinklera, J.W. Richardson Jr., S.M. McDeavitt, Actinide distribution in a stainless steel–15 wt% zirconium high-level nuclear waste form, J. Nucl. Mater. 279 (2000) 234–244.

[18] L.R. Bairi, S. Ningshen, U.K. Mudali, B. Raj, Microstructural analysis and corrosion behaviour of D9 stainless steel–Zirconium metal waste form alloys, Corros. Sci. 52 (2010) 2291–2302.

[19] L.R. Bairi, S. Ningshen, U.K. Mudali, B. Raj, Corrosion issues related to disposal of 316 SS-zirconium metal waste form under simulated repository conditions, Corros. Eng. Sci. Tech. 46 (2011) 171–176.

[20] L.R. Bairi, S. Ningshen, U.K. Mudali, B. Raj, Corrosion investigations on metal waste form alloys of titanium-modified Type 316 stainless steel-zirconium in simulated groundwater media, Corrosion 68 (2012) 784–792.

[21] W.L. Ebert, E. Buck, J. Fortner, Heat treatments of RAW-1 (Re), Argonne and Pacific Northwest National Laboratories, August 2011, FCRD-WAST-2011-000289.

[22] Atlas of Eh-pH diagrams: intercomparison of thermodynamic databases, National Institute of Advanced Industrial Science and Technology, Research Center for Deep Geological Environments, Naoto TAKENO, Geological Survey of Japan Open File, Report No. 419, 2005.

[23] N. Ramasubramanian, N. Preocanin, R.D. Davidson, Analysis of passive films on stainless steel by cyclic voltammetry and Auger spectroscopy, J. Electrochem. Soc. 132 (1985) 793–798.

[24] R. Wada, T. Nishimura, K. Fujiwara, M. Tanabe, M. Mihara, Experimental study on hydrogen gas generation rate from corrosion of Zircaloy and stainless steel under anaerobic alkaline conditions, in: Radioactive Waste Management and Environmental Remediation-ASME American Society for Mechanical Engineering, Fairfield, New Jersey, USA, 1999.

[25] C.F. Baes, R.E. Mesmer, The Hydrolysis of Cations, John Wiley and Sons, New York, 1976.